Novel structure of active platinum-bismuth site for oxidation of carbon monoxide

Bing Nan
Shanghai Institute of Applied Physics,Chinese Academy of Sciences
Qiang Fu
Shandong University https://orcid.org/0000-0002-6682-8527
Miao Shu
Shanghai Institute of Applied Physics
Lulu Zhou
Shandong University
Wei-Wei Wang
Shandong University
Chun-Jiang Jia
Shandong University https://orcid.org/0000-0002-4254-5100
Chao Ma
Hunan University https://orcid.org/0000-0001-8599-9340
Jun-Xiang Chen
TILON Group Technology Limited
Lina Li
Shanghai Synchrotron Radiation Facility
Rui Si (sirui@mail.sysu.edu.cn)
Shanghai Institute of Applied Physics

Article

Keywords: active platinum-bismuth site, carbon monoxide, oxidation

Posted Date: December 28th, 2020

DOI: https://doi.org/10.21203/rs.3.rs-123932/v1

Version of Record: A version of this preprint was published at Nature Communications on June 7th, 2021. See the published version at https://doi.org/10.1038/s41467-021-23696-7.

Abstract

As the technology development, the future advanced combustion engines must be designed to perform at a low temperature. Thus, it is a great challenge to synthesize high active and stable catalysts to resolve exhaust below 100 °C. Here, we report that bismuth as a dopant added to form platinum-bismuth cluster on silica for CO oxidation. The highly reducible oxygen species provided by surface metal-oxide (M-O) interface could be activated by CO at low temperature (~ 50 °C) with a high CO_2 production rate of 487 $\mu mol_{CO2} \cdot g_{Pt}^{-1} \cdot s^{-1}$ at 110 °C. Experiment data combined with density functional calculation (DFT) results demonstrate that Pt cluster with surface Pt–O–Bi structure is the active site for CO oxidation via providing moderate CO adsorption and activating CO molecules with electron transformation between platinum atom and carbon monoxide. These findings provide a novel and general approach towards design of potential outstanding performance catalysts for redox reaction.

Introduction

The CO oxidation reaction ($CO + 1/2\ O_2 = CO_2$) is a well-known model reaction in heterogeneous catalysis, as well as a key step to resolve automobile exhaust containing CO, NO and hydrocarbons[1–5]. Therefore, higher activity at lower temperatures with good stability, such as platinum-based catalysts, are in great demand. In order to pursue high catalytic performance for CO oxidation, a series of reducible oxides including CeO_2[2], FeO_x[3], MnO_2[4] and Co_3O_4[4] were used as active supports for Pt catalysts, due to their rich surface oxygen vacancy and the so-called “strong metal–support interaction”[6–8]. In another hand, irreducible oxide of commercial production, low cost and extensive application such as SiO_2 and Al_2O_3, usually showed poor ability to disperse active platinum species of ultra-small size (< 2 nm).

Many research groups have found that the addition of a secondary element, such as Sn[5], K[9], and Co[10], distinctly improved the activity of silica- or alumina-supported platinum catalysts, no matter in the form of oxide clusters or metallic alloy for Pt. Zhai et al. prepared partially oxidized Pt-alkali-$O_x(OH)_y$ species, which served as the active site for low temperature Pt-catalyzed water-gas shift reaction[9]. As for bismuth element, a high oxide ion conductivity dopant, has been reported to promote the transition metal (Co)[11] and noble metal (Pd)[12] catalysts for the CO oxidation reaction. However, the doping of bismuth to platinum usually focus on PtBi alloy or intermetallic compound[13,14]. So, it could be the first case to determine the formation of platinum-bismuth oxide cluster on silica with uniform Pt-O-Bi structure showing excellent thermal stability.

On the other hand, the precise determination of active site and reaction mechanism is still in arguments[12,15]. This promotion effect has been explained previously that bismuth oxide species could produce more oxygen vacancy to enhance the CO oxidation efficiency[11]. However, the local structure of active site for Bi-promoted catalyst and structure-function relationship in practical catalysts are still complicated, because of limited characterization techniques and complex active site structure. Therefore,

we employed the comprehensive characterization methods to investigate the local structure of platinum-bismuth cluster catalysts and confirm the active site of Pt–$[O]_x$–Bi structure.

Moreover, various interfaces in platinum-based catalysts have been illustrated key role in CO oxidation reactions, such as metal – support[3,16,17], metal – oxide[18–20] and metal – metal hydroxide[21]. Chen et al. reported iron nickel hydroxide-platinum nanoparticles (Pt-OH-Fe/Ni) were highly efficient for CO oxidation owing to abundant sites of Pt-OH-M interfaces[19]. However, these different interfaces are often unstable and difficult to establish precisely. Therefore, it is a big challenge to build up stable and specific interface to provide unique catalytic properties.

In this work, we prepared silica-supported platinum-bismuth catalysts via an incipient wetness impregnation, possessing excellent sinter resistance due to the formation of oxidized $Pt_xBi_yO_z$ cluster. The dopant of bismuth species constructure a unique interface between platinum and bismuth (Pt–$[O]_x$–Bi structure) species, which exhibits an absolutely different active site compared with pure platinum sample, providing superior active oxygen species activated by CO at low temperature (~ 50 °C) with a high CO_2 production rate of 487 $\mu mol_{CO2} \cdot g_{Pt}^{-1} \cdot s^{-1}$ at 110 °C. Meanwhile, this interface structure prevents oversaturated CO adsorption from poison of platinum species and activates CO molecules to catalyze CO oxidation in a lower apparent activation energy.

Results

Structural characterization of bismuth-doped platinum samples. A serial of silica-supported platinum and platinum-bismuth samples were prepared by a co-incipient wetness impregnation method. The bulk concentrations of platinum and bismuth (Pt: 0.8, 0.9 and 0.9 wt.%; Bi: 2.3 and 6.1wt.% for 1Pt-SiO_2, 1Pt2Bi-SiO_2, 1Pt5Bi-SiO_2 respectively) are close to these designed numbers, indicating the disposition of bismuth species have no effect on the loading of platinum (Supplementary Table 1). Furthermore, the Bi-free and Bi-doped samples have the similar textural properties, such as S_{BET} values and the type of adsorption-desorption isotherms (Supplementary Table 1 and Supplementary Fig. 1), in which we can exclude the physical effect on the following catalytic performance.

Small-size oxide species were extremely stable on silica surface in Bi-promoted samples in aberration-corrected high-angle annular dark-field imaging scanning transmission electron microscopy (HAADF-STEM) images (Fig. 1a,b), even after heat treatment in air. Only ultrafine clusters of 1.7±0.4 nm with narrow size-distribution were created in 1Pt2Bi-SiO_2 (Supplementary Fig. 2e,f and 3a), without any crystallized platinum or bismuth metal/oxide particles. However, after calcination in air, huge metallic Pt particles of ~ 100 nm (Supplementary Fig. 2a) and platinum oxide clusters (1.6±0.5 nm) simultaneously appeared in 1Pt-SiO_2 (Supplementary Fig. 2b,c and 3b). It illustrates that the addition of bismuth element could suppress the growth of metal/oxide particles, similar to the promotion by alkali ions[9] and silica support shows poor ability to stabilize platinum species. Furthermore, the corresponding aberration-corrected energy dispersive spectroscopy (EDS) mapping results of 1Pt2Bi-SiO_2 (Fig. 1c) show that

platinum and bismuth elements distribute uniformly at the cluster level within the same areas on the surface of SiO_2 without evident separation. Xie et al. also reported that bismuth species was deposited selectively on the Pt particles rather than the carbon support[22]. Meanwhile, the X-ray diffraction (XRD) also confirmed the promotion of bismuth species, in which no obvious $Pt/PtO/PtO_2/Bi/Bi_2O_3$ phase was detected in 1Pt2Bi-SiO_2, even in a “slow-scan” mode (Fig. 1d and Supplementary Fig. 4). When bismuth oxide species were deposited on silica separately (2Bi-SiO_2), it also stabilized in small-size without any diffraction peaks of Bi/Bi_2O_3 in XRD profiles (Fig. 1d). However, the observation of sharp Pt peaks (39.7º and 46.2º) verifies the formation of huge Pt particle in 1Pt-SiO_2. As shown in Fig. 1c, the dopant of bismuth species reaches optimization at 2 wt.% and the formation of broad diffraction peak of Bi_2O_3 for 1Pt5Bi-SiO_2. Therefore, bismuth oxide species as a promoter could improve the anti-sintering ability for platinum dispersed on an inert support.

The local coordination structure of platinum and bismuth species. According to aberration-corrected HAADF-STEM images, we can observe the existence of platinum-bismuth oxide clusters. X-ray absorption fine structure (XAFS) technique was applied to clarify the local structure of this cluster in Bi-promoted samples. The X-ray absorption near-edge structure (XANES) of Pt-L_3 edge profiles (Fig. 2a, Supplementary Table 2) showed platinum is in a low valence state (+ 1.8), due to the formation of huge metallic Pt particles in 1Pt-SiO_2. As the increasing of bismuth-dopant, the average oxidation state of platinum arises from 1.8 to 3.5, may due to bismuth oxide species could make interaction with platinum to stabilize abundant oxygen around Pt atom and thus enhancing average valance state of platinum. The extended X-ray absorption fine structure (EXAFS) fitting results (Fig. 2b and Supplementary Table 2) indicated that the major Pt − O ($R \approx 2.0$ Å, $CN \approx 5$) shell plus an apparent Pt − Bi ($R \approx 3.0$ Å, $CN \approx 4$) component originated from the Pt−$[O]_x$−Bi structure, further demonstrating the formation of homogeneous oxidized $Pt_xBi_yO_z$ cluster (Fig. 2e). Meanwhile, the XANES profiles of Bi−L_3 edge (Fig. 2c) and X-ray photoelectron spectroscopy (XPS) spectra display that bismuth species were in the pure Bi^{3+} state for Bi-promoted samples (Supplementary Fig. 5), which could exclude the possibility of PtBi alloy. While for 1Pt-SiO_2, without strong interaction between Pt and SiO_2, a dominant Pt − Pt metallic shell ($R \approx 2.8$ Å, $CN \approx 6.4$) from metallic Pt particle and a minor Pt − O−Pt shell ($R \approx 3.1$ Å, $CN \approx 2.7$) from small-size Pt_xO_z cluster could be determined. In addition, in-situ diffuse reflectance infrared Fourier transform spectroscopy (DRIFTS) experiments were frequently employed to detect the existence form of platinum species (single atoms, clusters or particles). As shown in Fig. 2d and Supplementary Fig. 6, only gases CO peaks was detected for 1Pt2Bi-SiO_2. However, for 1Pt-SiO_2-400 with almost identical oxide cluster size and loading amounts of platinum species (Supplementary Fig. 7) with 1Pt2BI-SiO_2, two CO adsorption peaks on $Pt^{\delta+}$ single atom (2093 cm^{-1}), oxide cluster (2075 cm^{-1})[23] were determined. It further evidences the formation of oxidized $Pt_xBi_yO_z$ cluster, which possesses totally different structural composition and adsorption capacity in Fig. 2e. To our best knowledge, it is the first time to observe the formation of uniform platinum-bismuth oxide clusters to suppress the aggregation of Pt species.

Catalytic performance of Pt/PtBi-SiO $_2$ catalysts in CO oxidation. CO oxidation was applied as a model reaction to investigate the role of bismuth-dopant. When the catalysts were pretreated at 300 °C under air, Bi-free and Bi-promoted samples shows almost same CO oxidation activity with complete CO conversion at ~ 220 °C (Supplementary Fig. 8), may due to poor ability to adsorb CO or overhigh valence of platinum species[24]. However, we found that hydrogen reduction significantly enhanced CO oxidation activity for Bi-promoted catalysts (Fig. 3a). The temperature of 50% CO conversion dropped off from 165 to 85 °C as the reduction temperature increasing from 0 to 210 °C. Interestingly, a platform appeared as hydrogen reduction at 150 and 180 °C, indicating a structure transformation of active site occurred during the hydrogen reduction compared with fresh Bi-doped catalysts. On the basis of the CO oxidation activity (Fig. 3b), a remarkable promotion to platinum-silica catalysts was observed by the addition of Bi oxide species with similar Pt loading (0.9 wt.%). The catalytic performance reaches the maximum at the dopant of 2 wt.% (Supplementary Fig. 9), may due to overmuch bismuth oxide species hindering CO adsorption or covering platinum active site. For comparison, pure Bi catalysts (2Bi-SiO_2) shows no CO oxidation activity below 160 °C (Fig. 3b), demonstrating bismuth species are not active site just as secondary dopant to modification platinum active site. Furthermore, we collected the kinetic data to compare the inherent catalytic activity. The specific activity normalized by the platinum amount for 1Pt2Bi-SiO_2 was 487 $\mu mol_{CO}\ g_{Pt}^{-1}\ s^{-1}$ at 110 °C, as active as the reported Pt/CeO_2 catalysts (103–518 $\mu mol_{CO}\ g_{Pt}^{-1}\ s^{-1}$ at 80–130 °C, see Table 1), as well as ten times higher than that of pure Pt catalyst (Supplementary Table 3). For eliminating size-effect on active site, 1Pt-SiO_2-400 was similarly inactive for CO oxidation at 100 °C reaction (Supplementary Fig. 9b), though possessing similar cluster size (1.2 ± 0.1 nm) to 1Pt2Bi-SiO_2 (Supplementary Fig. 7). It indicates that the dispersion of platinum species does not dominantly determines the CO oxidation activity. In another hand, the apparent activation energy (E_a) of Bi-promoted platinum catalysts (~52 kJ mol^{-1}) is similar to that of CeO_2-supported Pt catalyst (40 – 50 kJ mol^{-1})[2,25], and distinctly lower than that of pure 1Pt-SiO_2 (~70 kJ mol^{-1}) and other inert support platinum catalysts[5,26] (Fig. 3c). This may give a hint on the totally different reaction mechanism or active site for our Bi-promoted Pt-SiO_2 catalysts. Additionally, 1Pt2Bi-SiO_2 showed remarkable thermo-stability (Fig. 3d) and catalytic stability under the extremely high space velocity (300,000 $mL{\cdot}g_{cat}^{-1}{\cdot}h^{-1}$, Supplementary Fig. 9c).

Structural characterization of used Pt/PtBi-SiO $_2$ catalysts. After CO oxidation, we employed a comprehensive characterization to determine the actual structure of active site. The aberration-corrected HAADF-STEM images (Fig. 4a-c and Supplementary Fig. 10) showed that the platinum species were still in the formation of cluster (~ 2 nm) without any visible lattice fringes of crystal Pt/PtO/PtO_2 component after CO oxidation. Meanwhile, the related STEM-EDS mapping results indicated that the Pt and Bi elements still distribute together (Fig. 4d and Supplementary Fig. 11). Thus, the bismuth element around platinum cluster still make an interaction with platinum species to prevent aggregation of clusters into huge particles, even after hydrogen reduction. The EXAFS fitting results in Supplementary Fig. 12 indicated the Pt–$[O]_x$–Bi can be maintained after hydrogen pretreatment at 210 °C without air exposure during the whole test process. In another hand, there is an obvious aggregation of platinum cluster (~

3.0 nm) compared to fresh 1Pt-SiO_2 (~ 1.7 nm) in Supplementary Fig. 10c. Mahmudov and co-workers found obvious aggregation of platinum particles on activated carbon after hydrogen reduction[27]. The XRD results in Fig. 4e also confirmed the huge metallic platinum particles were still maintained in 1Pt-SiO_2 with sharp diffraction peaks at 39.7º and 46.2º. In contrast, no obvious diffraction peaks of Pt/PtO/PtO_2 phases were detected in Bi-promoted samples, further confirming the high dispersion of platinum species. There was a broad peak of Bi_2O_3 in 1Pt5Bi-SiO_2, due to the aggregation of bismuth species.

Furthermore, we employed XAFS technique to detect the valance state and local coordination structure of active sites. XANES data in Fig. 4f indicated platinum species are at low valence state after CO oxidation: 1Pt5Bi-SiO_2 (1.3) > 1Pt2Bi-SiO_2 (0.7) > 1Pt-SiO_2 (0.4) (Supplementary Table 2) due to hydrogen reduction, indicating lower oxidized state of Pt species are appropriate for lower temperature CO oxidation[24,28]. In order to require more reliable local coordination structure for used Bi-promoted samples, we conducted the EXAFS fitting process with or without Pt−O−Bi shell in Supplementary Fig. 13. Obviously, Pt−O−Bi shell is an essential composition to acquire the best fitting results. The EXAFS fitting results for Pt − Pt shell with $CN \approx 8$ also confirmed the average grain size of platinum cluster was ~ 2 nm for 1Pt2Bi-SiO_2[29] as observed in HAADF-STEM images (Fig. 4a-c). In addition, minor Pt − O ($R \approx 2.0$ Å, $CN \approx 1.2 - 2.2$) plus Pt − O−Bi ($R \approx 3.0$ Å, $CN \approx 2.2$) composition was detected (Fig. 4e, Supplementary Table 2), due to the existence of Pt−$[O]_x$−Bi structure. Thus, the clusters in 1Pt2Bi-SiO_2 observed in aberration-corrected HAADF-STEM images (Fig. 4a-c) was metallic platinum cluster. In another hand, the XANES and XPS profiles in Fig. 4h,i indicated that bismuth species were still in oxidative state even after hydrogen reduction and CO oxidation, which can exclude the formation of PtBi alloy. For pure platinum catalyst, only a metallic Pt − Pt shell ($R \approx 2.76$ Å, $CN \approx 10$) was fitted for 1Pt-SiO_2 without apparent Pt − O shell, which may result in low activity due to no surface-active oxygen to participate in CO oxidation[30]. As a reference, 1Pt-SiO_2-400 exhibited low activity in CO oxidation, even though possessing similar local coordination structure for Pt − O and Pt − Pt shell to the used 1Pt2Bi-SiO_2 (Supplementary Fig. 14b). Thus, we can draw a conclude that the surface Pt−$[O]_x$−Bi structure plays a key role in low temperature CO oxidation reaction rather than oxidized Pt_xO_z cluster.

The reducibility and active oxygen for Pt/PtBi-SiO_2. As we known, the reducibility of catalysts is crucial in various redox reactions[31−33]. For fresh samples, a main reduction peak located at ~ 100 °C appeared on profiles of H_2−temperature programmed reduction (H_2−TPR) in Fig. 5a for 1Pt-SiO_2 contributed by the reduction of Pt_xO_z clusters[34]. However, for Bi-doped samples, the first broad reduction peak was shifted to 162 °C (1Pt2Bi-SiO_2) and 197 °C (1Pt5Bi-SiO_2) in Supplementary Fig. 15a, due to the strong interaction of Pt − O−Bi[35], as confirmed by EXAFS fitting results. The hydrogen consumption values (Supplementary Table 5) increased for 107 μmol/g (1Pt-SiO_2) to 185 μmol/g (1Pt2Bi-SiO_2). Although the doping of bismuth oxide species can enhance the surface oxygen, there is no promotion in CO oxidation due to over strong interaction (Pt − O−Bi) cannot release oxygen atom to take part in reaction. CO−temperature programmed reduction (CO−TPR) results in Supplementary Fig. 16 also demonstrated the surface-active

oxygen for 1Pt2Bi-SiO_2 (~ 75 μmol/g) is almost two times than that (~ 40 μmol/g) of 1Pt-SiO_2. However, these oxygen species only reacted with CO molecule above 100 °C, well consistent with low activity in CO oxidation with oxidative pretreatment (Supplementary Fig. 8).

We also carried out the H_2−TPR and CO−TPR experiments for used Pt/PtBi-SiO_2 samples after CO oxidation without air exposure absolutely to detect reducibility and active oxygen of active site. For H_2−TPR experiments, no reduction peak below 200 °C appeared in 1Pt-SiO_2 due to the use of hydrogen reduction treatment before reaction. However, a broad reduction peak starting from 50 °C still existed in Bi-doped samples, indicating the existence of Pt−$[O]_x$−Bi structure. It indicates the new active site of platinum cluster with surface Pt−$[O]_x$−Bi structure exhibits more reducible property. Additionally, CO−TPR results of used 1Pt2Bi-SiO_2 also evidenced these surface oxygen atoms in Pt−$[O]_x$−Bi structure was superior active to react with CO molecule generating CO_2 from ~ 50 °C (Fig. 5b), well consistent with the CO oxidation “light off” temperature (Fig. 3b). However, 1Pt-SiO_2 did not activate the surface hydroxyls to produce CO_2 (water-gas shift reaction) until 195 °C[9]. This highly reducible oxygen species may motivate initial CO oxidation (~ 50 °C) through Mars-van Krevelen (MvK) mechanism[36] and show a strong correlation between reaction rate and active oxygen amount in Fig. 5c. Therefore, the Pt−$[O]_x$−Bi structure with low valance state of $Pt^{\delta+}$ ($0<\delta<2$) species in the used Bi-promoted samples provides superior active oxygen species to catalyze preliminary stage of CO oxidation.

The CO adsorption on Pt−$[O]_x$−Bi active site. Despite the identification of active site structure in silica-supported platinum-bismuth catalysts being important, the adsorption of reaction gas is a more key factor for catalytic behavior. We further intend to investigate the CO adsorption on Pt−$[O]_x$−Bi structure for Bi-promoted catalysts. The in-situ DRIFTS experiments displayed that CO adsorption intensity of Bi-promoted sample is moderate compared to that of pure platinum sample (Fig. 6a), indicating the surface Pt−$[O]_x$−Bi structure could prevent oversaturated adsorption of CO molecule (CO poison) on Pt clusters or nanoparticles, just like the reported alkali-doped Pt catalysts[9]. The CO adsorption reached saturation rapidly for 1Pt-SiO_2 at 2062 cm^{-1} attributed to linear CO adsorbed on Pt^0 sites (Pt^0−CO)[37] (Fig. 6a and Supplementary Fig. 17), resulting in no other Pt sites dissociating gases oxygen into active oxygen species[38]. However, the peak for CO adsorption over 1Pt2Bi-SiO_2 was detected at 2043 cm^{-1}, which was absolutely different linear CO adsorbed on Pt^0 sites. This red-shift phenomenon can be eliminated the possibility of either size-effect of Pt species or CO adsorption on pure Bi species. In one hand, 1Pt-SiO_2-400 with total platinum cluster also showed the peak around 2060 cm^{-1} (Supplementary Fig. 18) similar with the peak (2062 cm^{-1}) in 1Pt-SiO_2. In another hand, there is no CO adsorption peak for 2Bi-SiO_2 except for gases CO peaks (Supplementary Fig. 19), no matter with oxidative or reduced pretreatment. Therefore, the low-frequency band at 2043 cm^{-1} is attributed to CO molecules adsorbed on the new active site (Pt−$[O]_x$−Bi), even less doping of bismuth species (Supplementary Fig. 20), and this may result from the unique local coordination structure of Pt−$[O]_x$−Bi structure or electron transfer from platinum atom to CO molecule[39,40]. Panagiotopoulou and co-workers reported that the alkali additives to Pt/TiO_2

catalyst generate a low-frequency shoulder band (~ 2030 cm^{-1}) resulting in strengthen of Pt – CO bond[40]. Furthermore, when the oxygen was introduced, the activated CO molecule adsorbed on Pt–$[O]_x$–Bi structure could be converted to CO_2 quickly (~135 s) and completely (Fig. 6b). Our density functional theory (DFT) calculation builds up various simulation model for Pt@PtO_x without and with Bi dopant (Supplementary Fig. 21) and the corresponding calculated vibrational frequencies of a CO molecule adsorbed on different sites. The vibration peaks at 2062 cm^{-1} and 2043 cm^{-1} in the experiments were attributed to the configurations in Supplementary Figs. 21c,f respectively. One can see that upon the doping of the Bi atoms, the number of the Pt-O bonds had decreased. It is not surprising since Bi atoms are oxophilic and can seize O atoms from Pt. In Supplementary Fig. 22, we presented the density of states (DOS) for the *d* electrons of the Pt atom (Supplementary Figs. 21c,f) on which the CO molecule adsorbs. As the coordination number of the Pt atom decreases, the center of the *d* band becomes closer to the Fermi level, corresponding to strengthened activity. Thus, due to the unique structure of Pt–$[O]_x$–Bi, more electron was transformed from Pt atom to CO molecules to activated carbon monoxide, resulting in the red-shift on CO adsorption band in DRIFTS experiments.

Additionally, we, employed in-situ DRIFTS experiments with a mode: “CO adsorption → reaction conditions (1 vol.% CO/20 vol.% O_2/N_2 flow) at 200 °C → CO adsorption” to detect the stability of active site. For 1Pt2Bi-SiO_2, the Pt–$[O]_x$–Bi structure could be maintained after CO oxidation (2042 cm^{-1}), well consistent with the band after hydrogen pretreatment at 210 °C (Fig. 6c). For 1Pt-SiO_2, after CO oxidation, the CO adsorption band occurred a blue shift (2072 cm^{-1}) compared to the band (2062 cm^{-1}) after hydrogen reduction at 210 °C (Supplementary Fig. 23), due to the surface oxidation of metallic Pt cluster.

Discussion

In summary, we have prepared silica-supported platinum-bismuth catalysts via an incipient wetness impregnation, possessing excellent sinter resistance due to the formation of oxidized $Pt_xBi_yO_z$ cluster. The Bi-promoted catalysts exhibit an absolutely different active site for platinum cluster with surface Pt–$[O]_x$–Bi structure compared with pure platinum sample, providing superior active oxygen species activated by CO at low temperature (~ 50 °C) with a high CO_2 production rate of 487 $\mu mol_{CO2} \cdot g_{Pt}^{-1} \cdot s^{-1}$ at 110 °C. Even after hydrogen reduction, the surface Pt–$[O]_x$–Bi structure still stabilizes platinum cluster in cluster-scale with unique properties: (1) preventing oversaturated CO adsorption from poison of platinum species; (2) activating CO molecules to catalyze CO oxidation in a lower apparent activation energy. Therefore, we have provided a general approach towards design of potential active and stable platinum catalysts.

Table 1
Comparison of the activities over the representative platinum catalysts for the oxidation of carbon monoxide.

	Temp (°C)	Gas feed composition	r_1	r_2	Apparent activation energy (kJ/mol)	Ref
Inert support						
1wt.%Pt/θ-Al_2O_3	200	3.7%CO/3.7%O_2/He	0.7	72	–	41
0.2 wt%Pt/m-Al_2O_3	200	2.5% CO/2.5% O_2/Ar	0.2	118	78	15
0.5wt.%Pt/SiO_2	200	40TorrCO/100TorrO_2/He	1.3	256	95	4
Reducible support						
1 wt.% Pt/CeO_2	225	2%CO/1%O_2/N_2	8.7	871	55	14
1.1 wt%Pt/TiO_2	140	1%CO/10%O_2/N_2	2.9	261	–	42
0.5wt.%Pt/MnO_2	200	40TorrCO/100 Torr O_2/He	5.5	1107	66	4
0.5wt.%Pt/Fe_2O_3			1.7	349	70	
0.5wt.%Pt/CeO_2			6.9	1384	63	
1 wt%Pt/CeO_2	134	0.4%CO/10%O_2/He	1.0	103	43	2
1 wt%Pt/CeO_2	80	1.9%CO/1.2%O_2/He	5.2	518	30	43
0.22Pt/CeO_2	110	1%CO/20%O_2/He	0.2	92	–	18
Our results						
1Pt2Bi-SiO_2	90	1%CO/20%O_2/N_2	1.7	210	50	This work
	100		3.1	390		
	110		3.9	487		
	175	2%CO/1%O_2/N_2	9.1	1138	47	
	200		15.6	1953		
	225		58.3	7289		

r_1: Reaction rate by catalyst weight ($\mu mol_{CO} \cdot g_{cat}^{-1} \cdot s^{-1}$); r_2: Reaction rate by Pt amount ($\mu mol_{CO} \cdot g_{Pt}^{-1} \cdot s^{-1}$)

Methods

Catalyst preparation. SiO_2 was calcination at 400 °C for 4 h (ramping rate: 2 °C/min) to remove surface water before catalysts preparation. Deposition of platinum, and bismuth onto the SiO_2 support was carried out by a co-incipient wetness impregnation. Firstly, a solution of $Bi(NO_3)_3$ (50–124 mg respective) and $Pt(NH_3)_4(NO_3)_2$ (20 mg) in 0.1 mol/L HNO_3 solutions (3 mL) was added dropwise onto SiO_2 power (1 g) under manually stirring. The powders were standing in ambient conditions for 2 h and then dried in still air at 80 °C for 12 h, followed by air-calcination at 550 °C for 4 h (ramping rate: 2 °C/min). As comparison, we also prepared 1Pt-SiO_2 calcinated at 400 ºC, 1Pt1Bi-SiO_2 and 2Bi-SiO_2 samples with same synthetic method. The Bi and Pt contents were controlled on demand during preparation process of catalysts, and the data of these catalysts is as follows:

1Pt-SiO_2 (1 wt. % Pt, 0 wt. % Bi),

1Pt2Bi-SiO_2 (1 wt. % Pt, 2 wt. % Bi),

1Pt5Bi-SiO_2 (1 wt. % Pt, 5 wt. % Bi)

2Bi-SiO_2 (2 wt. % Bi)

1Pt-SiO_2-400 (1 wt. % Pt)

1Pt1Bi-SiO_2 (1 wt. % Pt, 1 wt. % Bi)

Catalytic activity tests. The CO oxidation activities for the PtBi-SiO_2 samples were evaluated in a plug flow reactor using 30 mg of sieved (20–40 mesh) powders in a gas mixture of 1 vol.% CO/20 vol.% O_2/N_2 (from Jinan Deyang Corporation, 99.997% purity) at a flow rate of 67 mL/min giving a gas hourly space velocity (GHSV) of ~134,000 $mL \cdot g_{cat}^{-1} \cdot h^{-1}$. The catalysts were pretreated in 5% H_2/N_2 (50 mL/min) at 210 °C for 30 min before reaction with 10 $ºC \cdot min^{-1}$. After the catalysts cooled down to room temperature under a flow of pure N_2 gas, reactant gases were passed through the reactor. The outlet gas compositions of CO and CO_2 were monitored online by nondispersive IR spectroscopy (Gasboard 3500, Wuhan Sifang Company, China). CO conversion was defined as $CO_{reaction}$ / CO_{input} × 100%. The related stability tests were done in the same conditions at the constant reaction temperature of 100ºC for 10 h with a GHSV of ~134,000 $mL \cdot g_{cat}^{-1} \cdot h^{-1}$. Rate measurements were made in the separate catalytic tests rather than the “light-off” mode, i. e. the same gas composition, but at specific space velocities to ensure operation in the kinetic regime (< 20% conversion of CO).

Materials characterization. The actual platinum and bismuth concentrations of the catalysts were analyzed by inductively coupled plasma atomic emission spectroscopy (ICP-AES; Optima 5300DV,

PerkinElmer). The air-calcined samples (fresh catalysts) were used directly for characterization. First, 0.1 g catalyst (accurate to 0.0001 g) was added to 2 mL hydrofluoric acid under continuous stirring until the powder was dissolved adequately. Second, the as-formed SiF_4 was removed via evaporation. Then, almost 3 mL of nitric acid was introduced and the solution was kept slightly boiling for 2 h. Finally, the solution was cooled to nearly 25 ºC and diluted for the ICP-AES test.

XRD patterns were recorded on a Bruker D8 Advance diffractometer (40 kV, 40 mA) with a scanning rate of 4° min^{-1}, using Cu $K_{\alpha 1}$ radiation (λ = 1.5406 Å). The diffraction patterns were collected from 10 to 80° with a step of 0.02°. The 2θ angles were calibrated with a μm-scale Alumina disc. The powder sample after grinding was placed inside a quartz sample holder for each test. XPS analysis was performed on an Axis Ultra XPS spectrometer (Kratos, U.K.) with 225 W of Al *K*α radiation. The C 1 s line at 284.8 eV was used to calibrate the binding energies.

The nitrogen adsorption-desorption measurements were performed on an ASAP 2020-HD88 analyzer (Micromeritics Co. Ltd.) at 77 K. The measured powders were degassed at 250 °C under vacuum (< 100 μmHg) for over 4 h. The BET specific surface areas (S_{BET}) were calculated from data in the relative pressure range between 0.05 and 0.20. The pore diameter (D_p) distribution was calculated from the adsorption branch of the isotherms, based on the BJH method.

The TEM and high-resolution TEM (HRTEM) experiments were carried out on a FEI Tecnai G^2 F20 microscope operating at 200 kV. All the tested samples were suspended in ethanol, and then a drop of this dispersed suspension was placed on an ultra-thin (3–5 nm in thickness) carbon film-coated Cu grid. The as-formed sample grid was dried naturally under ambient conditions before loaded into the TEM sample holder. The aberration-corrected HAADF-STEM images were carried out on a JEOL ARM200F microscope equipped with probe-forming spherical-aberration corrector.

XAFS experiments Pt L_3 (E_0 = 11564.0 eV) and Bi L_3 (E_0 = 13419.0 eV) edge was performed at BL14W1 beamline of Shanghai Synchrotron Radiation Facility (SSRF) operated at 3.5 GeV under “top-up” mode with a constant current of 260 mA. The XAFS data were recorded under fluorescence mode with a Lytle detector for Pt/PtBi-SiO_2 samples. Only X-ray absorption near edge structure (XANES) data of Bi L_3 edge was collected due to the similar edge energies of Bi and Pt L_3 edge. The energy was calibrated accordingly to the absorption edge of pure Pt and Bi foil. Athena and Artemis codes were used to extract the data and fit the profiles. For the XANES part, the experimental absorption coefficients as function of energies $\mu(E)$ were processed by background subtraction and normalization procedures. Based on the normalized XANES profiles, the molar fraction of Pt^{4+}/Pt^0 and Bi^{3+}/Bi^0 can be determined by the linear combination fit with the help of various references (Pt foil for Pt^0, PtO_2 for Pt^{4+}, Bi foil for Bi^0 and Bi_2O_3 for Bi^{3+}). For the extended X-ray absorption fine structure (EXAFS) part, the Fourier transformed (FT) data in *R* space were analyzed by applying PtO_2 and metallic Pt model for Pt–O and Pt–Pt contributions. The passive electron factors, S_0^2, were determined by fitting the experimental data on Pt and Bi foils, and fixing the coordination number (*CN*) of Pt–Pt and Bi–Bi to be 12, and then fixed for further analysis of the

measured samples. The parameters describing the electronic properties (e.g., correction to the photoelectron energy origin, E_0) and local structure environment including coordination number (*CN*), bond distance (*R*) and Debye-Waller factor around the absorbing atoms were allowed to vary during the fit process. To distinguish the effect of Debye-Waller factor from coordination number, we set σ^2 to be 0.0030 and 0.0080 Å^2 for all the analyzed Pt–O and Pt–Pt shells, according to the fitted results of Pt foil and PtO_2 standards. We also set σ^2 to be 0.008 Å^2 for all the analyzed Pt–Bi paths, considering that the *Z* number of Bi (83) is close to that of Pt (78). To distinguish the effect of correction to the photoelectron energy origin from distance, we set ΔE_0 to be 11.3, 13.3 and 14.1 eV for fresh 1Pt-SiO_2, 1Pt2Bi-SiO_2 and 1Pt5Bi-SiO_2, respectively, which were obtained from the linear combination fits on XANES profiles and the fitting results of Pt foil (ΔE_0 = 8.3±1.2 eV) and bulk PtO_2 (ΔE_0 = 15.0±0.9 eV) standards and the ΔE_0 for all used samples is 7.4±1.8 eV according to EXAFS fitting results. The samples with pretreatment in 5 vol. % H_2/He at 210 °C for 30 min was reduced in reactor with ball valves for air blocking and make the sample tablets in glovebox filled with N_2 for whole process before XAFS test.

In-situ DRIFTS. It was carried out in a diffuse reflectance cell (Harrick system) equipped with CaF_2 windows on a Bruker Vertex 70 spectrometer using a mercury-cadmium-telluride (MCT) detector cooled with liquid nitrogen. In a typical steady test, the powder sample (ca. 20 mg) was pretreated in air (21 vol % O_2/79 vol % N_2) at 300 °C or in hydrogen gas (5 vol. % H_2/He) at 210 °C for 30 min and cooled to room temperature under pretreatment atmosphere (30 mL min^{-1}). Then a background spectrum was collected via 32 scans at 4 cm^{-1} resolution. The reaction gas with 1% CO/20% O_2/79% N_2 was introduced into the in-situ chamber (30 mL min^{-1}) and heated in a stepped way (every 40 K); DRIFTS spectra were obtained by subtracting the background spectrum from subsequent spectra. The IR spectra for every step were recorded continuously for 40 min to reach the equilibrium. Analysis of the spectra has been carried out by using OPUS software. For further investigation of the process of adsorption-desorption of CO over Pt/PtBi-SiO_2 catalysts, a "CO – N_2–CO – O_2" test was measured with in situ DRIFTS. The process of activation was carried out as described above. Then a background spectrum was collected at a certain temperature (100 °C) under pure N_2 (30 mL min^{-1}). The catalyst was exposed continuously to 2% CO in N_2 for CO adsorption for 30 min. Once CO gas was switched to an N_2 stream, also the corresponding IR spectra were recorded for 30 min. Then the catalyst was exposed to 2% CO in N_2 for CO re-adsorption for 30 min; ultimately 1% O_2 in an N_2 stream was introduced, in order to follow the surface changes during the CO removal process. The CO adsorption for Pt/PtBi-SiO_2 samples was also carried out in the mode "CO adsorption → CO oxidation at 200 °C → CO adsorption" to detect structure evolution of adsorption site after CO oxidation.

DFT calculations. First-principles calculations were performed within the framework of the density functional theory (DFT) using the Vienna ab initio simulation package (VASP)[44, 45]. The projector augmented wave (PAW) method was employed[46], and the wave functions were expanded by plane-wave basis sets with an energy cutoff of 400 eV. The exchange-correlation effects were described by the

optPBE-vdW functional[47,48], which explicitly takes Van der Waals interactions into account. The simulation model of the PtO_x system was constructed by nesting an icosahedral Pt_{55} cluster inside a platinum oxide layer that contains 32 Pt atoms and 66 O atoms, and the deposited Bi atoms (10 atoms in the model) were placed on the outer layer of the platinum oxide. The unit cell contains enough vacuum along all three directions to eliminate spurious interactions between periodic images. Since the model of the system is an isolated cluster, the first Brillouin zone was sampled using the Γ point only. In the geometry optimizations, all atoms were allowed to relax until the maximum force was below 0.03 Å /eV. The vibrational frequencies of CO were calculated through a finite differential approach, in which only the CO adsorbate, the Pt atom that connects it, and the surrounding Pt, O and Bi atoms were allowed to move while all other atoms were kept frozen.

Reducible property and surface oxygen. Hydrogen temperature-programmed reduction (H_2–TPR) was applied to determine the pretreatment temperature under hydrogen and reducibility. The measurements were carried out on a Micromeritics Autochem II 2920 instrument. Fresh (as calcinated in air) catalysts were used for characterization. Prior to the measurement, the catalyst (20–40 mesh, ~ 100 mg) was pretreated for 30 min in a flow of 5% O_2/He (30 mL·min^{-1}) at 300 ºC (10 ºC·min^{-1}). The test was carried out from room temperature to 600 ºC (10 ºC·min^{-1}) at a ramp of 10 ºC·min^{-1} under 5% H_2/He (30 mL·min^{-1}). A thermal conductivity detector (TCD) was used to detect the changes of hydrogen concentration. The in situ H_2-TPR for used samples was also performed on Autochem II 2920 instrument after CO oxidation without air exposure with He purging to remove reactant gas completely.

Carbon monoxide Temperature-programmed reduction (CO–TPR) experiments using CO as reductant were performed on Micromeritics Autochem II 2920 instrument with mass spectrometer (Tilon GRP Technology Limited LC-D200M) to detect the active oxygen species in fresh and used samples. The fresh sample (100 mg, 20–40 mesh) was pretreated in 5% O_2/He (30 mL·min^{-1}) at 300 ºC (10 ºC·min^{-1}) for 30 min. The used samples after CO completely conversion was conducted for CO–TPR without air exposure and then cooling down to 30 ºC and switching to He (50 mL·min^{-1}) for 10 min to remove reactant gas (CO and O_2 molecules). Finally, the sample was heated from room temperature to 500 ºC with a step of 5 ºC·min^{-1} under a mixture gas flow of 5% CO/He (20 mL·min^{-1}). During the measurement, the signals of He (m/z = 4), CO_2 (m/z = 44), H_2O (m/z = 18, 17), CO (m/z = 28, 16), and H_2 (m/z = 2) were detected. The reported CO_2 and H_2 data were normalized by dividing by the corresponding He standard signal (m/z = 4).

Declarations

Data availability

All data generated or analysed during this study are included in this published article (and its Supplementary Information files) or can be obtained from the authors upon reasonable request.

Competing interests

The authors declare no competing interests.

Author contributions

B.N. developed platinum-bismuth catalysts, tested for catalytic activity, and prepared the article. M.S. carried out the TEM/HRTEM images for all catalysts. L.L.Z. and W.W.W. measured in-situ DRIFTS data. Q.F. made the DFT calculations. L.N.L. carried out XAS measurements and analyzed the data. C.M. carried out the aberration-correction HAADF-STEM and EDS mapping images of all catalysts. J.X.C performed the CO−TPR experiments. R.S. and C.J.J. conceived and supervised the project, procured funds, and wrote the manuscript, with contributions from all authors.

Acknowledgments

This work was supported by “National Key Basic Research Program of China” (2017YFA0403402); “Project of the National Natural Science Foundation of China” (21773288, U1932119, 21771117 and 21805167), the Taishan Scholar Project of Shandong Province of China, and the Young Scholars Program of Shandong University. This work was also supported by shanghai large Scientific facilities center.

References

1. Liu, W. & Flytzani-Stephanopoulos, M. Total oxidation of carbon monoxide and methane over transition metal-fluorite oxide composite catalysts . Catalyst composition and activity. *J. Catal.* **153**, 304-316 (1995).
2. Nie, L. et al. Activation of surface lattice oxygen in single-atom Pt/CeO_2 for low-temperature CO oxidation. *Science* **358**, 1419-1423 (2017).
3. Qiao, B. T. et al. Single-atom catalysis of CO oxidation using Pt_1/FeO_x. *Nat. Chem.* **3**, 634-641 (2011).
4. An, K. et al. Enhanced CO oxidation rates at the interface of mesoporous oxides and Pt nanoparticles. *J. Am. Chem. Soc.* **135**, 16689−16696 (2013).
5. Michalak, W. D. et al. CO oxidation on PtSn nanoparticle catalysts occurs at the interface of Pt and Sn oxide domains formed under reaction conditions. *J. Catal.* **312**, 17−25 (2014).
6. Nan, B. et al. Effects of Multiple Platinum Species on Catalytic Reactivity Distinguished by Electron Microscopy and X-ray Absorption Spectroscopy Techniques. *J. Phys. Chem. C* **121**, 25805−25817 (2017).
7. Deelen, T. W., Mejía, C. H. & Jong, K. P. Control of metal-support interactions in heterogeneous catalysts to enhance activity and selectivity. *Nat. Catal.* **2**, 955−970 (2019).
8. Acerbi, N., Tsang, S. C. E., Jones, G., Golunski, S. & Collier, P. Rationalization of interactions in precious metal/ceria catalysts using the d-band center model. *Angew. Chem. Int. Ed.* **52**, 7737 −7741

(2013).

9. Zhai, Y. P. et al. Alkali-stabilized Pt-OH_x species catalyze low-temperature water-gas shift reactions. *Science* **329**, 1633–1636 (2010).
10. Xu, H., Fu, Q., Guo, X. G. & Bao, X. H. Architecture of Pt–Co bimetallic catalysts for catalytic CO oxidation. *ChemCatChem* **4**, 1645–1652 (2012).
11. Lou, Y. et al. The effects of Bi_2O_3 on the CO oxidation over Co_3O_4. *Catal. Today* **175**, 610–614 (2011).
12. Ma, D.-D. et al. Promoting effect of bismuth oxide on Pd for low temperature CO oxidation. *ChemCatChem* **9**, 499–504 (2017).
13. Kim, Y. T., Shin, D. S., Park, Y. K. & Choi, I.-H. Effects of Bi-Pt alloy on electrical characteristics of Pt/$SrBi_2Ta_2O_9$/CeO_2/Si ferroelectric gate structure *J. Appl. Phys.* **86**, 3387 (1999).
14. Zhang, D. T. et al. One-step, facile and ultrafast synthesis of phase- and size-controlled Pt-Bi intermetallic nanocatalysts through continuous-flow microfluidics. *J. Am. Chem. Soc.* **137**, 6263–6269 (2015).
15. Shang, Z. et al. Activity and stability of Co_3O_4-based catalysts for soot oxidation: The enhanced effect of Bi_2O_3 on activation and transfer of oxygen. *Appl. Catal. B* **209**, 33–44 (2017).
16. Wang, W.-W. et al. Crystal plane effect of ceria on supported copper oxide cluster catalyst for CO oxidation: importance of metal–support interaction. *ACS Catal.* **7**, 1313–1329 (2017).
17. Du, P.-P. et al. Effect of strongly bound copper species in copper-ceria catalyst for preferential oxidation of carbon monoxide. *Appl. Catal. A* **518**, 87–101(2016).
18. Zhu, H. Y. et al. Constructing hierarchical interfaces: TiO_2-supported PtFe-FeO_x nanowires for room temperature CO oxidation. *J. Am. Chem. Soc.* **137**, 10156–10159 (2015).
19. Weng, Z. et al. Metal/oxide interface nanostructures generated by surface segregation for electrocatalysis. *Nano Lett.* **15**, 7704–7710 (2015).
20. Peng, L. S. et al. Chimney effect of the interface in metal oxide/metal composite catalysts on the hydrogen evolution reaction. *Appl. Catal. B* **245**, 122–129 (2019).
21. Chen, G. X. et al. Interfacial effects in iron-nickel hydroxide–platinum nanoparticles enhance catalytic oxidation. *Science* **344**, 495–499 (2014).
22. Xie, J. H. et al. Influence of dioxygen on the promotional effect of Bi during Pt-catalyzed oxidation of 1,6-Hexanediol. *ACS Catal.* **6**, 4206–4217 (2016).
23. Chen, Y. et al. Identifying size effects of Pt as single atoms and nanoparticles supported on FeO_x for the water-gas shift reaction. *ACS Catal.* **8**, 859–868 (2018).
24. Jeong, H. et al. Controlling the oxidation state of Pt single atoms for maximizing catalytic activity. *Angew. Chem. Int. Ed.* **59**, 20691–20696 (2020).
25. Jones, J. et al. Thermally stable single-atom platinum-on-ceria catalysts via atom trapping. *Science* **353**, 150–154 (2016).

26. Zhang, Z. L. et al. Thermally stable single atom Pt/m-Al_2O_3 for selective hydrogenation and CO oxidation. *Nat. Commun.* **8**, 16100 (2017).
27. Mahmudov, R., Shu, Y.Y., Rykov, S., Chen, J. G. & Huang, C. P. The reduction of perchlorate by hydrogenation catalysts. *Appl. Catal. B* **81**, 78–87 (2008).
28. Ke, J. et al. Strong local coordination structure effects on subnanometer PtO_x clusters over CeO_2 nanowires probed by low-temperature CO oxidation. *ACS Catal.* **5**, 5164–5173 (2015).
29. 29. Frenkel, A. I., Hills, C. W. & Nuzzo, R. G. A view from the inside: complexity in the atomic scale ordering of supported metal nanoparticles. *Phys. Chem. B* **105**, 12690–12703 (2001).
30. Uner, D., Tapan1, N.A., Özen, I. & Üner, M. Oxygen adsorption on Pt/TiO_2 catalysts. *Appl. Catal. A* **251**, 225–234 (2003).
31. Choi, J., Zhang, S. H. & Hill, J. M. Reducibility and toluenehydrogenation activity of nickel catalysts supported on γ-Al_2O_3 and κ-Al_2O_3. *Catal. Sci. Technol.* **2**, 179–186 (2012).
32. Zedan, A. F., Mohamed, A. T., El-Shall, M. S., AlQaradawi, S. Y. & AlJaber, A. S. Tailoring the reducibility and catalytic activity of CuO nanoparticles for low temperature CO oxidation. *RSC Adv.* **8**, 19499–19511 (2018).
33. Lei, Q. et al. Influence of cerium precursors on the structure and reducibility of mesoporous CuO-CeO_2 catalysts for CO oxidation. *Appl. Catal. B* **119–120**, 308–320 (2012).
34. Zhu, S. H. et al. SiO_2 promoted Pt/WO_x/ZrO_2 catalysts for the selective hydrogenolysis of glycerol to 1,3-propanediol. *Appl. Catal. B* **158**, 391–399 (2014).
35. Lan, M. L. et al. Chemoselective hydrogenation of 3-nitrostyrene to 3-aminostyrene over Pt-Bi/TiO_2 catalysts. *Mol. Catal.* **432**, 23–30 (2017).
36. Wang, C. L. et al. Water-mediated Mars-Van Krevelen mechanism for CO oxidation on ceria-supported single-atom Pt_1 catalyst. *ACS Catal.* **7**, 887–891 (2017).
37. Brieger, C. et al. A combined in-situ XAS–DRIFTS study unraveling adsorbate induced changes on the Pt nanoparticle structure. *J. Catal.* **339**, 57–67 (2016).
38. Ding, K. L. et al. Identification of active sites in CO oxidation and water-gas shift over supported Pt catalysts. *Science* **350**, 189–192 (2015).
39. Liu, A. N. et al. Getting insights into the temperature-specific active sites on platinum nanoparticles for CO oxidation: a combined in situ spectroscopic and ab initio density functional theory study. *ACS Catal.* **9**, 7759–7768 (2019).
40. Panagiotopoulou, P. & Kondarides, D. I. Effects of alkali additives on the physicochemical characteristics and chemisorptive properties of Pt/TiO_2 catalysts. *J. Catal.* **260**, 141–149 (2008).
41. Moses-DeBusk, M. et al. CO oxidation on supported single Pt atoms: experimental and ab initio density functional studies of CO interaction with Pt atom on θ-Al_2O_3(010) surface. *J. Am. Chem. Soc.* **135**, 12634–12645 (2013).

42. Zhou, Y. et al. Photothermal catalysis over nonplasmonic Pt/TiO_2 studied by operando HERFD-XANES, resonant XES, and DRIFTS. *ACS Catal.* **8**, 11398–11406 (2018).
43. Pereira-Hernández, X. I. et al. Tuning Pt-CeO_2 interactions by high-temperature vapor-phase synthesis for improved reducibility of lattice oxygen. *Nat. Commun.* **10**, 1358 (2019).
44. Kresse, G. & Furthmüller, J. Efficiency of ab-initio total energy calculations for metals and semiconductors using a plane-wave basis set. *Comput. Mater. Sci.* **6,** 15–50 (1996).
45. Kresse, G. & Furthmüller, J. Efficient iterative schemes for ab initio total-energy calculations using a plane-wave basis set. *Phys. Rev. B* **54,** 11169–11186 (1996).
46. Blöchl, P. E. Projector augmented-wave method. *Phys. Rev. B* **50,** 17953–17979 (1994).
47. Dion, M., Rydberg, H., Schröder, E., Langreth, D. C. & Lundqvist, B. I. Van der Waals density functional for general geometries. *Phys. Rev. Lett.* **92**, 246401 (2004).
48. Klimeš, J., Bowler, D. R. & Michaelides, A. Chemical accuracy for the van der Waals density functional. *J. Phys.: Condens. Matter* **22**, 022201 (2010).

Figures

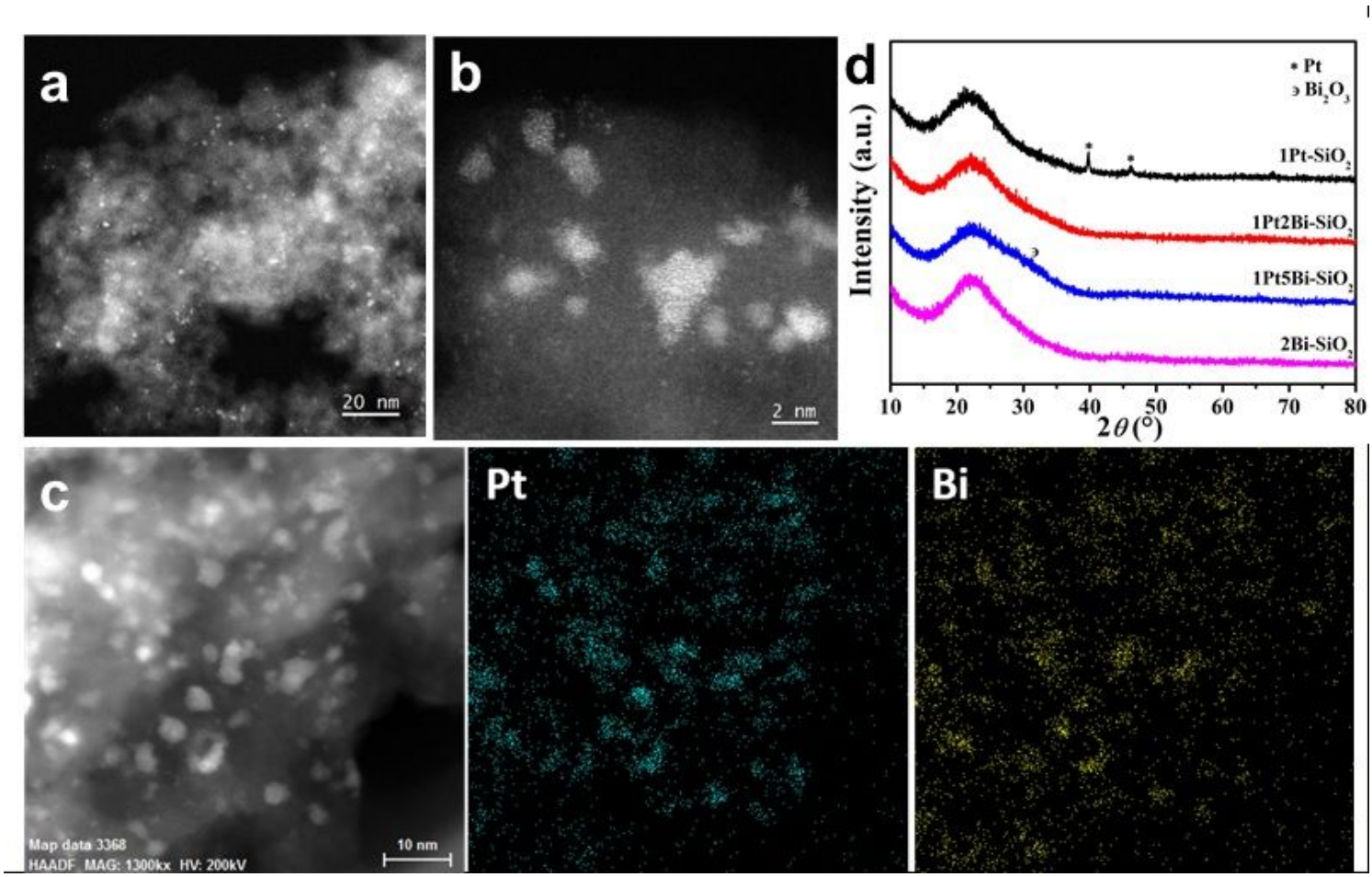

Figure 1

Structural characterization of Pt/PtBi-SiO2 samples. Representative aberration-corrected HAADF-STEM images (a,b) at different scales and corresponding STEM-EDS elemental mapping images (c) for fresh 1Pt2Bi-SiO2; XRD patterns (d) of fresh Pt/PtBi-SiO2 samples.

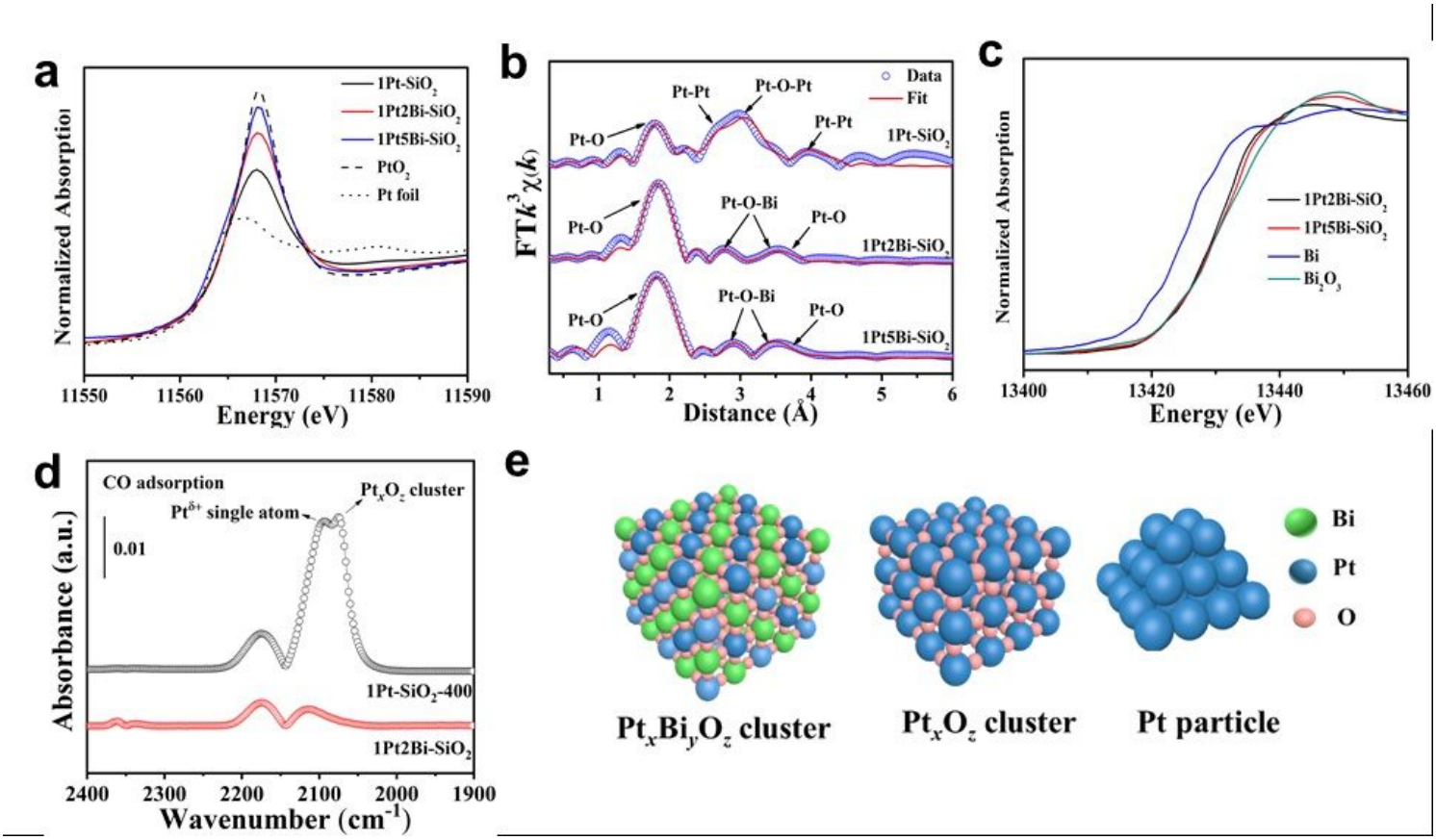

Figure 2

Local coordination structure of Pt/PtBi-SiO2 samples. Pt L3–edge (a) XANES profiles, (b) EXAFS fitting results in R space and Bi L3–edge (c) XANES profiles of Pt/PtBi-SiO2 samples; (d) in-situ DRIFTS experiments for CO adsorption of 1Pt2Bi-SiO2 and 1Pt-SiO2-400; (e) Schematic demonstration on platinum-bismuth oxide clusters, platinum oxide clusters and metallic Pt particles.

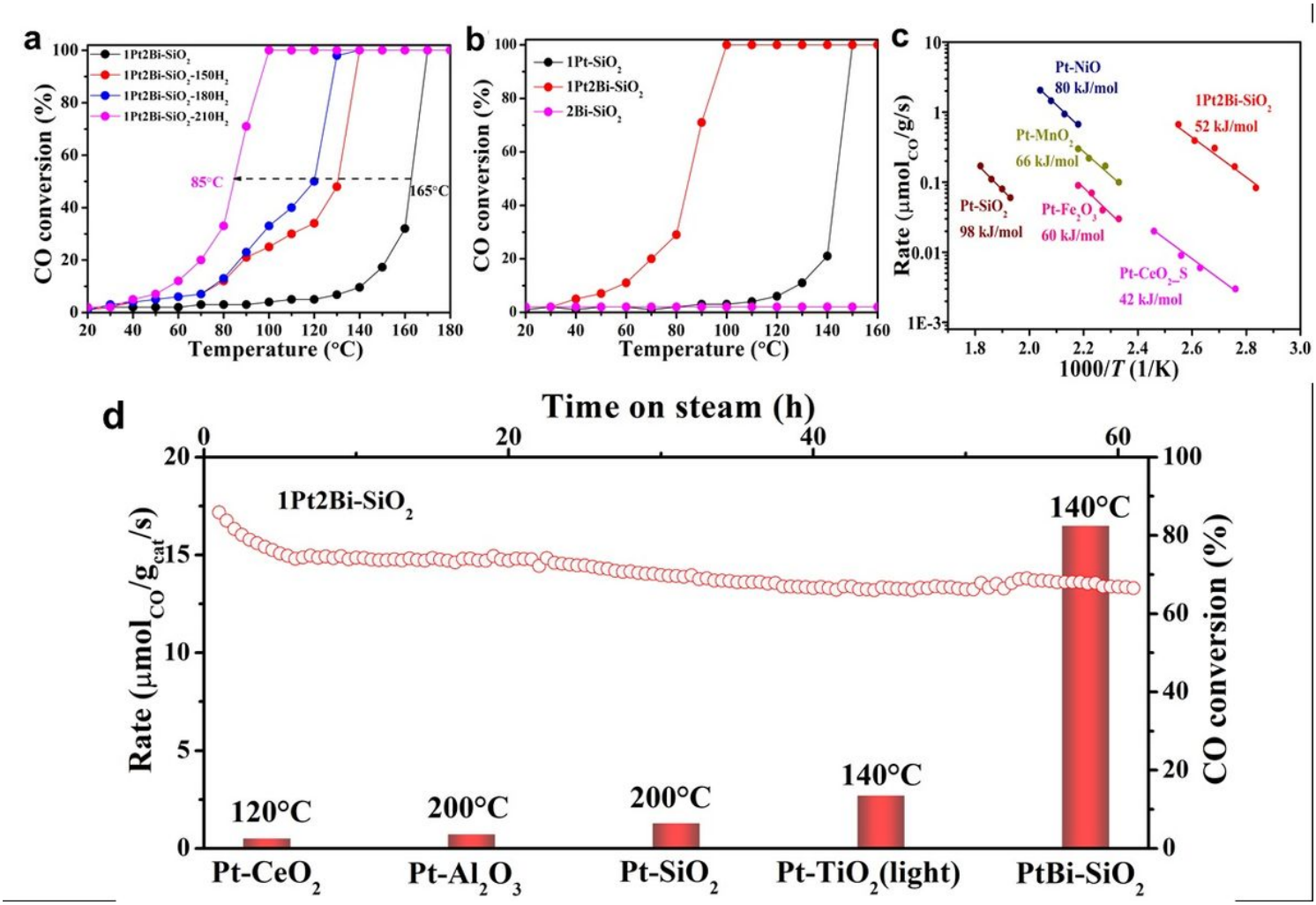

Figure 3

Catalytic performance of Pt/PtBi-SiO2 catalysts in CO oxidation. (a) CO oxidation experiments with different H2-pretreatment temperature for 1Pt2Bi-SiO2; (b) Catalytic CO oxidation light-off performance of different catalysts at a gas hourly space velocity of 134,000 mL gcat−1 h−1 in 1 vol.% CO/20 vol.% O2/79 vol.% N2. Temperature ramp: 2 °C min-1; (c) Apparent activation energy (Ea) of various catalysts; (d) CO oxidation stability test (150 °C, 200,000 mL g-1 h-1) and reaction rate of different catalysts.

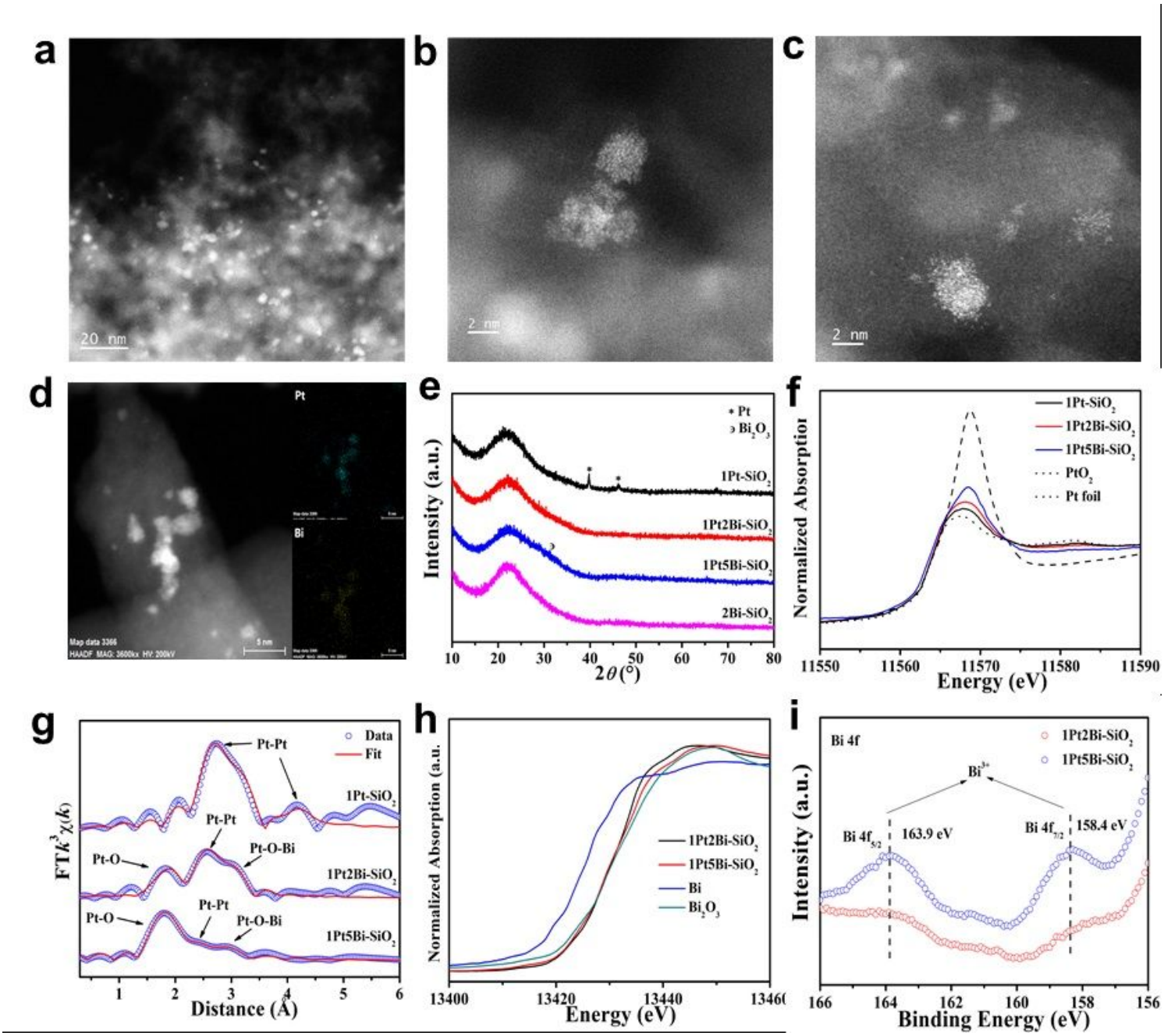

Figure 4

Structural characterization of used Pt/PtBi-SiO2 catalysts. Representative aberration-corrected HAADF-STEM images of (a-c) for used 1Pt2Bi-SiO2 at different scales and (d) the corresponding EDS element mapping of used 1Pt2Bi-SiO2; (e) XRD patterns of used Pt/PtBi-SiO2 samples; Pt L3–edge (f) XANES profiles and (g) EXAFS fitting results in R space and Bi L3–edge (h) XANES and (i) XPS profiles of Pt/PtBi-SiO2 samples.

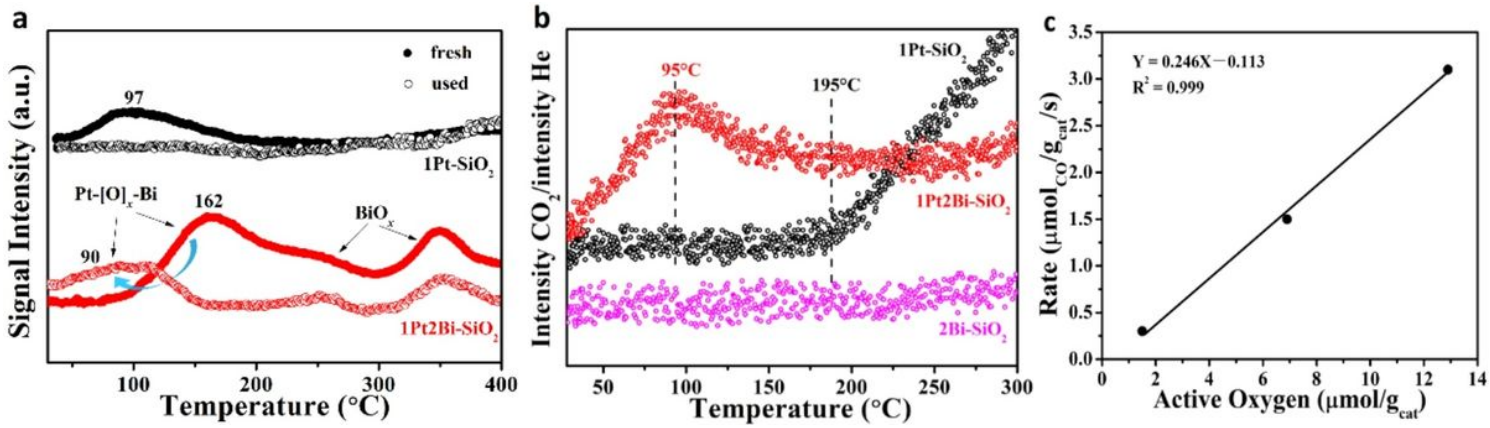

Figure 5

The reducible property and active oxygen for Pt/PtBi-SiO2. (a) H2-TPR profiles of fresh Pt/PtBi-SiO2 catalysts and used catalysts after CO oxidation without exposure to air; (b) in-situ CO-TPR of used Pt/PtBi-SiO2 samples after CO oxidation without exposure to air; (c) linear equation for active oxygen vs reaction rate for used Pt/PtBi-SiO2 samples.

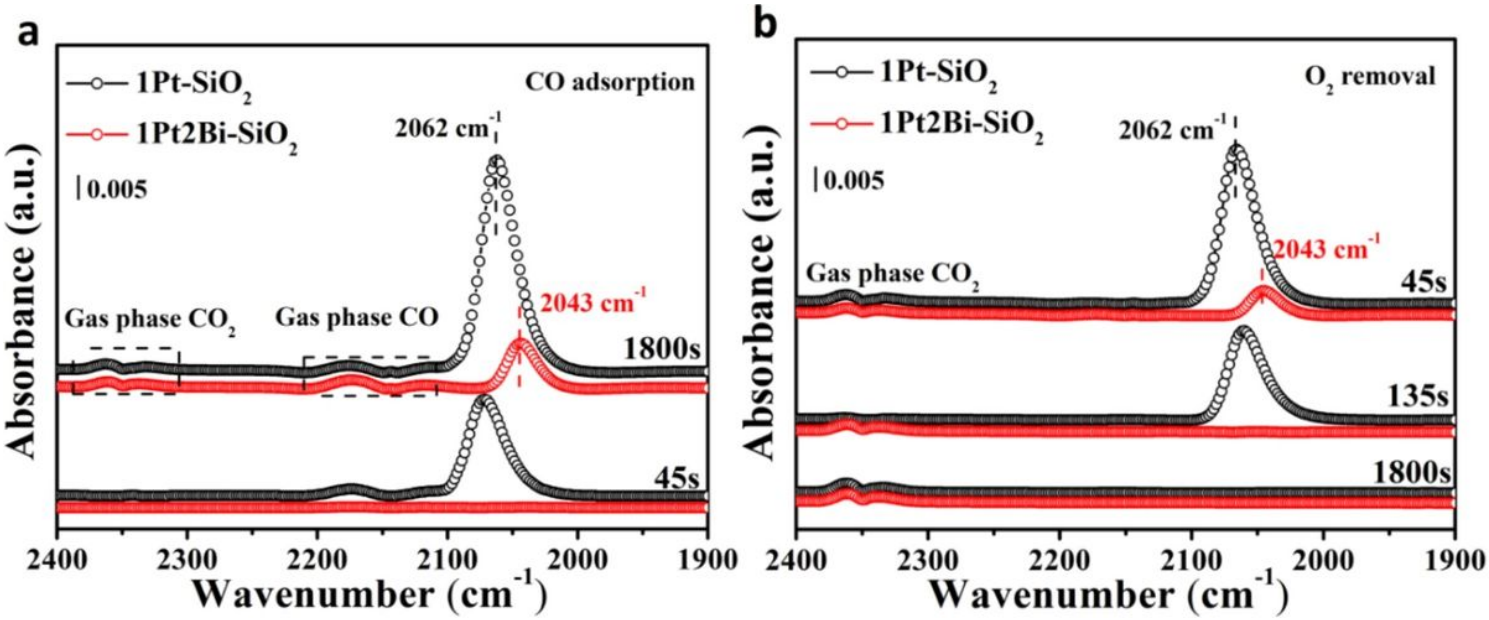

Figure 6

The CO adsorption on Pt-[O]x-Bi active site. In-situ DRIFTS study of (a) CO adsorption and (b) O2 removal on Pt/PtBi-SiO2 samples; (c) In-situ DRIFTS in the mode: “CO adsorption → reaction conditions (1% CO/ 20% O2/N2 flow) at 200°C → CO adsorption” on 1Pt2Bi-SiO2 without catalyst replacement and air exposure. (The catalysts were pretreated in situ at 210 °C under H2 flow in the DRIFTS reaction cell before data collection; CO flow rate: 30 mL min−1; catalyst mass: 20 mg; temperature: 100 °C).

Supplementary Files

This is a list of supplementary files associated with this preprint. Click to download.

- NCSI.docx